Letter Vol. 45, No. 5 / 1 March 2020 / Optics Letters 1059

400 m rolling-shutter-based optical camera communications link

Elizabeth Eso,[1] Shivani Teli,[2] Navid Bani Hassan,[3] Stanislav Vitek,[2] Zabih Ghassemlooy,[1,4] and Stanislav Zvanovec[2]

[1]Optical Communication Research Group, Northumbria University Newcastle, UK
[2]Faculty of Electrical Engineering, Czech Technical University in Prague, Prague, Czech Republic
[3]Department of Physics, University of Strathclyde, Glasgow, UK
[4]QIEM, HI, Chinese Academy of Sciences, Quanzhou, China
*Corresponding author: elizabeth.eso@northumbria.ac.uk

Received 6 December 2019; accepted 12 January 2020; posted 17 January 2020 (Doc. ID 385423); published 18 February 2020

In this Letter, we develop a novel technique, to the best of our knowledge, to increase the link span (L_s) of a rolling shutter (RS)-based optical camera communications (OCC) system by reducing the spatial bandwidth of the camera in the out-of-focus regions. We demonstrate a 400 m line-of-sight RS-based OCC link, which is to date the longest L_s reported in these systems, and develop a detection method to extract the information out of the video frames, successfully. The proposed system relaxes the condition of a large surface area for the transmitter light source. Consequently, we show that at 400 m L_s and exposure times of 100–80 μs, a data rate of 450 bps is achieved successfully.

https://doi.org/10.1364/OL.385423

Optical camera communications (OCC) is considered as a pragmatic form of visible light communications (VLC), which utilizes an image sensor (IS) (i.e., cameras) as the receiver (Rx) and light-emitting diodes (LEDs), laser diodes (LDs), and liquid crystal displays as the transmitter (Tx) [1,2]. In OCC, the camera captures two-dimensional data in the form of image sequences, thus enabling multidimensional data transmission over the free-space channel. OCC offers multiple functionalities of vision, data communications, and localization, which can be used in a number of applications including all-optical Internet of Things (OIoT) [3,4]. OIoT-based applications include device-to-device communications, mobile attocells, vehicle-to-everything (V2X), smart environments, etc. [2], which releases the needed radio frequency spectrum for use in areas most required. Inspired by IoT, the Internet of Vehicles (IoV) is currently of high interest within the research community [4]. Recently, the widespread use of LEDs as tail-lights, brake lights, headlights, and street and traffic lights has opened up the potential opportunities for implementation of the intelligent transportation systems (ITS) to mitigate traffic congestion and therefore improve quality of life and the economy [2]. In addition, the availability of cameras in traffic networks, security surveillance, vehicles, etc., can be effectively exploited as an optical Rx, thus enabling the implementation of VLC-OCC links.

One of the advantages of camera-based Rxs over photodiodes is the higher signal-to-noise ratio (SNR) due to longer exposure time (T_{exp}) and larger overall photosensitive area, which results in longer link distances. OCC can be deployed in ITS for vehicle-to-vehicle, infrastructure-to-vehicle, and vehicle-to-infrastructure (V2I) communications; therefore, a long link span helps to establish a robust system [2,5]. The complementary-metal-oxide-semiconductor (CMOS)-based rolling shutter (RS) camera, which sequentially (row by row) integrates light illuminating the pixels thus operating similarly as scanning function, can be used to increase the data rate (R_b) higher than the frame rate (R_f) of the camera [6]. In Ref. [7], global-shutter (GS)-based OCC with a R_b of 15 bps over a link range of 328 m was reported for use in smart city applications with ∼4% wrongly decoded received bit streams. In Ref. [8], a RS-based OCC link for outdoor application with a maximum link span of 120 m, a bit error rate (BER) of $> 10^{-2}$ (at 120 m), and an achieved maximum R_b of 200 bps at a 4 m link span was reported. Further research on long-distance OCC links (beyond 120 m) using RS is yet to be investigated, to the author's best knowledge.

In order to establish long-distance VLC, there are a number of options including large-area light sources with high-power (meeting the eye safety), multiple light sources, wide-area optical Rx (at cost of reduced bandwidth), and multiple Rxs (i.e., cameras). In Ref. [7], a large-sized Tx with a dimension of 48 × 48 cm^2 was used. However, using a large Tx is impractical; therefore, in this Letter, we propose a novel reception technique in order to increase the transmission link span of RS-based OCC by reducing the camera's spatial bandwidth in the out-of-focus areas. This helps to have a larger footprint of the light source on the IS without reducing the field of view (FoV). We also develop a detection algorithm to effectively extract the received information from captured video frames. Previous works reported on OCC have used mainly cameras in the focused mode. However, cameras can also be used in their defocused modes depending on applications, e.g., indoor non-line-of-sight (LOS) communications or V2I-VLC [9]. We have

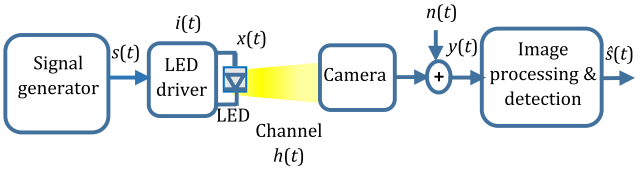

Fig. 1. Schematic block diagram of the long-distance OCC link.

used a light source (i.e., 2.5 × 2.5 cm^2) that is 19 times smaller than the source that was adopted in Ref. [7]. The proposed system is attractive in distance critical applications requiring relatively low R_b as in ITS (e.g., exchange of safety and traffic messages and positioning-related information) for smart traffic management. In this work, we achieve a communication link of up to 400 m with 100% success rate in data transmission achieving a R_b of 450 bps. The demonstrated system, to the best of our knowledge, is the longest link span achieved for a RS-based OCC link.

The block diagram of the proposed system is shown in Fig. 1. At the Tx, on–off keying non-return to zero (OOK-NRZ) data $s(t)$ are used for intensity modulation of the LED [a 2.5 × 2.5 cm^2 size chip on board (COB)] via the LED driver. The intensity-modulated light $x(t)$ is transmitted over a free-space channel and captured at the Rx using a CMOS RS camera with a 1000 mm telephoto lens. For the LOS link, the received signal is given by [10]

$$y(t) = \eta x(t) \circledast h(t) + n(t), \tag{1}$$

where $h(t)$ is the combined impulse response of the channel and camera, η is the quantum efficiency of the IS, and $n(t)$ is the additive white Gaussian noise including the ambient light-induced shot noise and the noise in the camera (i.e, fixed pattern, thermal, photocurrent shot, and flicker noise sources) [11]. The channel DC gain for the LOS link can be obtained as [10]

$$H(0)_{\mathrm{LOS}} = \begin{cases} \frac{A_{\mathrm{Tx-img}}(m+1)}{2\pi d_L^2}\cos^m(\Phi) g(\theta) T_s(\theta), & 0 \le \theta \le \xi \\ 0, & \theta > \xi \end{cases}, \tag{2}$$

where $A_{\mathrm{Tx-img}}$ is the area of the projected illuminated light source on the IS, d_L is the distance between the Tx and the camera's lens, and $T_s(\theta)$ and $g(\theta)$ are the gains of the optical filter and optical concentrator, respectively. Φ denotes the irradiance angle, ξ is the FoV semi-angle of the camera, and m represents Lambertian order of emission of the Tx. The incidence angle $\theta = \phi_{\mathrm{tilt}} + \sin^{-1}[(H_{\mathrm{Tx}} - H_{\mathrm{Rx}})/d_L]$, while the Rx tilt angle and heights of the Tx and Rx are denoted as ϕ_{tilt}, H_{Tx}, and H_{Rx}, respectively.

Usually, CMOS camera sensors (adopted as the Rx in this work) use the RS readout method, such that each pixel row is exposed in a row-by-row sequential manner with a fixed time delay (row readout time T_r). Moreover, in RS-based cameras, the exposure of each row takes place before the readout and not all at once, as in the case of GS-based cameras. Consequently, each pixel row's exposure does not commence at the same time. This is an advantage in OCC systems, which can lead to increased R_b higher than the camera's R_f, but at the cost of reduced coverage distance; hence, we propose a new technique to extend this coverage distance. Note that with RS-OCC, a flicker-free transmission is achievable; hence, we employ this technique in this work.

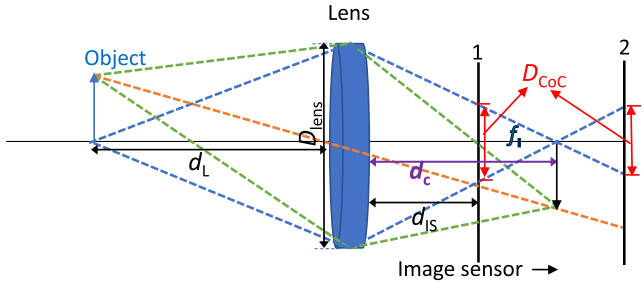

Fig. 2. Example of lens, image sensor, and object configuration.

Note that in OCC, the captured Tx's focused image size decreases with the increasing link span as given by the relationship $d_{\mathrm{img}} = d_{\mathrm{Tx}} f/d_L$, where d_{Tx} and d_{img} are the diameter of the Tx and the diameter of the projected Tx's image on the IS at the focal length f of the lens in use, respectively. This therefore constitutes a limitation for RS-based OCC links, as the received signal area on the IS of the camera, which determines the number of rows N_{rows} (i.e., the ON and OFF states of the Tx) obtainable, decreases with the increasing transmission distance. Consequently, we reduce this limitation by operating the camera in its out-of-focus (defocused) mode. Figure 2 shows a lens, object, and IS configuration. The IS could be moved from position 1 to 2 where varying sizes of the projected object's image are obtainable. Importantly, we use the defocusing feature of the camera, i.e., by altering the distance between the 1000 mm telephoto lens and the IS, to allow the Tx's image to converge beyond the focal point, whereby a larger footprint of the Tx is obtained.

Consequently, more N_{rows} are visible [detectable by the Rx (camera)], as illustrated in Fig. 3 for the defocused modes. Note that defocusing of the camera results in a disc-shaped pattern known as a circle of confusion (CoC), which is convoluted with the image as given by [12]

$$G_o(x, y) = G_i(x, y) \circledast\circledast G_{\mathrm{CoC}}(x, y), \tag{3}$$

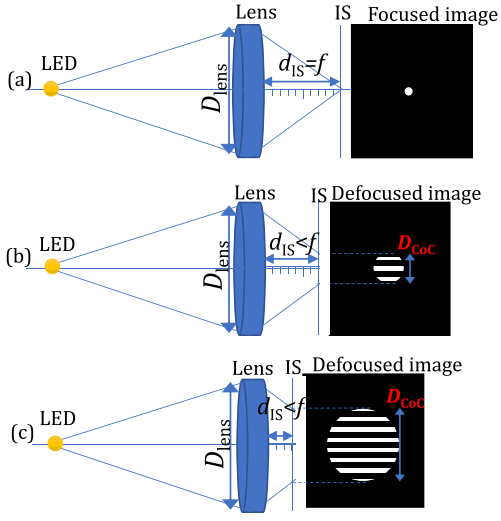

Fig. 3. Examples of width of captured Tx images on IS based on varying lens and IS configurations.

where $G_o(x, y)$ and $G_i(x, y)$ are the defocused and focused image intensity functions, respectively. $\circledast\circledast$ is the two-dimensional convolution operator, and $G_{\mathrm{CoC}}(x, y)$ is the CoC disc function, which is the same shape as the camera's lens aperture. For a circular aperture, we have [12]

$$G_{\mathrm{CoC}}(x, y) = U\left(\sqrt{x^2 + y^2}\right) - U\left(\sqrt{x^2 + y^2} - 0.5 D_{\mathrm{CoC}}\right), \tag{4}$$

and the diameter of CoC, D_{CoC}, is the same as the width of the defocused image of a point source and is given as [12]

$$D_{\mathrm{CoC}} = \frac{D_{\mathrm{lens}}}{2d_c}|d_c - d_{\mathrm{IS}}|, \tag{5}$$

where U(.) is the Heaviside step function, $D_{\mathrm{lens}} = f/f_{\mathrm{stop}}$ is the diameter of the lens aperture, f_{stop} is the focal stop number of the lens aperture, d_{IS} is the distance between the center of the lens to the IS, and d_c represents the distance between the center of the lens and the image, which can be obtained as [12]

$$d_c = \frac{d_L f}{d_L - f}. \tag{6}$$

Note that the size of CoC depends on the aperture diameter D_{lens} for collecting the light rays of d_{IS} and d_c. Consequently, to increase defocusing (i.e., D_{CoC}) in order to have the best signal area, $|d_c - d_{\mathrm{IS}}|$ must be maximized, and lower values of f_{stop} should be used to obtain larger D_{lens}. However, the amount of achievable defocusing is limited to the camera's optics design configuration. Figure 4 illustrates the N_{rows} as a function of the transmission distances for focused and three different defocused image modes for d_{IS} of f, $0.3f$, $0.5f$, and $0.7f$, $f = 1000$ mm and $D_{\mathrm{lens}} = f/10$, and width of rows = 0.05 cm. The N_{rows} increases with d_{IS}, e.g., at d_L of 20 m, the N_{rows} has increased from two for the focused image mode to 33, 52, and 71 for d_{IS} of $0.7f$, $0.5f$, and $0.3f$, respectively, thus enabling longer RS-OCC link spans. The width of one row in pixels (representing one bit or symbol for a fixed camera pixel clock) [13], $w_b = 1/(2f_{\mathrm{Tx}}T_r)$, where f_{Tx} denotes the Tx's switching frequency. Note that the N_{rows} increasing with the defocusing is at the cost of reduced light intensity level per pixel [i.e., lower peak SNR (PSNR)/pixel], since the received light is spread over a higher number of pixels. Interestingly, the latter can be compensated for by increasing the gain parameter of the camera (i.e., its sensitivity), the aperture size, and T_{exp} (within the required bandwidth) so as to capture more light but only to the extent that the rows still remain distinctive and not mixed up. In addition, a robust image processing algorithm (Fig. 5) is proposed to enhance the success rate of received bits.

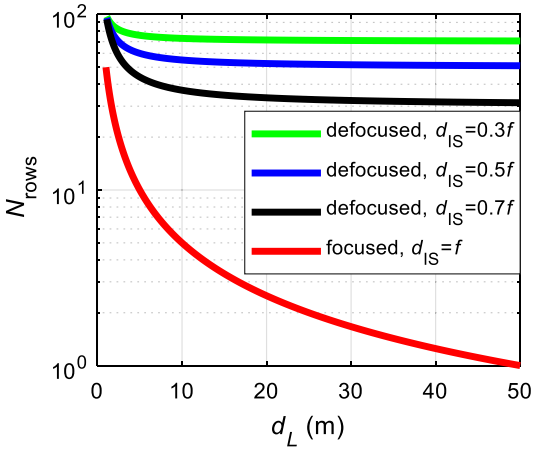

Fig. 4. N_{rows} versus d_L for a range of d_{IS}.

Consequently, at the Rx side, the output of the camera (IS) is processed off-line in MATLAB. As portrayed in the detection flowchart (Fig. 5), every video frame is converted from the red, green, and blue (RGB) color format to grayscale for both calibration and data videos after pixelation (i.e., digitizing the image to obtain the intensity/pixel value). The data videos are the captured transmitted data, whereas the captured calibration videos are the template shape of the Tx, which is used for equalization or otherwise described as the intensity compensation of the data video frames. Next, the region of interest (ROI) is selected (i.e., the footprint of the light source on the IS, which is the CoC) and then averaged over the rows to form a column vector. In order to avoid noise amplification at the start and end of the pixel rows in each frame, at least 10-pixel rows are eliminated from the top and bottom of the CoC. The received signal is then up-sampled to increase the resolution of the received signal. The correlation between the transmitted and received signal is carried out to determine the delay between them in order to extract the required received samples. A matched filter (MF) (via postprocessing in MATLAB) is applied to recover the data. The recovered data bits vector is then compared with the transmitted data to ascertain the success rate of received bits by determining the ratio of the wrongly decoded bits to the total number of transmitted bits (i.e., BER).

The system configuration and experimental setup for the long-distance OCC are shown in Fig. 6. The Tx was located on the sixth floor (height of 25 m), and the Rx was placed outdoors at a height of 1.40 m above the ground. At the start of the measurement campaign, the weather was partly cloudy/sunny while by the end it was sunny, with a temperature range of 23°C–25°C and wind speed and humidity of 2–6 mph and 51%–65%, respectively. The key experimental parameters include the LED

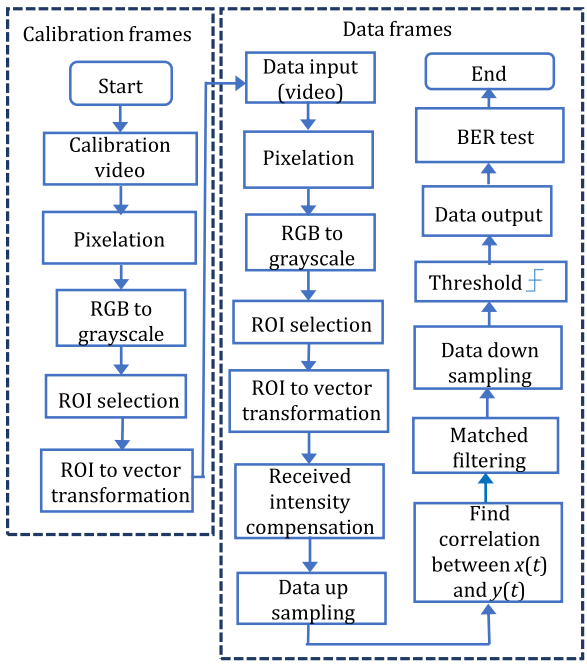

Fig. 5. Flowchart of detection.

drive current, FoV, and m, which are 0.33 A, 122°, and 0.96, respectively. The Tx data packet is 18 bits, the Rx's R_f is set to 25 fps for all experimental configurations considered, and the number of received data bits is ~32 per frame. The Rx's video resolution, pixel size, lens aperture, and f are 648 × 484 (RGB32), 2.2 × 2.2 μm^2, $f/10$, and 1000 mm, respectively. Measurements were carried out for a range of link spans L_s and T_{exp} of 150 to 400 m and 100 to 800 μs, respectively. Image frames of the transmitted data were captured with up to 100% success rate of received bits for all links considered in this work. In order to quantify the link performance for each L_s, we used the image quality metric of PSNR, which is given as [14]

$$P_{\text{SNR}} = 10 \log \frac{I_{\text{max}}^2}{\epsilon(i)}, \tag{7}$$

where I_{max} is the maximum possible pixel value, $I_{\text{max}} = 2^n - 1$, $n = 8$ for a grayscale image, and $\epsilon(i)$ is the pixel luminance mean squared error, which is defined by

$$\epsilon(i) = \frac{1}{N_{\text{rows}}} \sum_{1}^{N_{\text{rows}}} (I_{\text{Tx}}(i) - I_{\text{Rx}}(i))^2. \tag{8}$$

$I_{\text{Tx}}(i)$ and $I_{\text{Rx}}(i)$ are the difference between pixel and average pixel values for transmitted and received symbols (1 and 0), respectively, while i represents the row's index number. Figure 7 shows the PSNR versus L_s for a range of T_{exp}. As illustrated, PSNR improves with T_{exp} and decreases with the increasing L_s, e.g., for T_{exp} of 800 μs, PSNR drops by 2.1 dB when increasing L_s from 200 to 400 m. The maximum values of PSNR are 3.3 and 0.2 dB for T_{exp} of 800 μs and 100 μs at L_s of 150 m, respectively.

We have developed a novel technique to increase the link span of RS-based OCC by reducing the spatial bandwidth of the camera in the out-of-focus regions. The experimental analysis of the proposed scheme demonstrates a 100% success rate of received bits for a L_s of up to 400 m using a small surface area Tx of 2.5 × 2.5 cm^2. The choice of the T_{exp} played a key role in determining the value of PSNR. To the best of the authors' knowledge, no works have been reported for long-distance OCC links using RS.

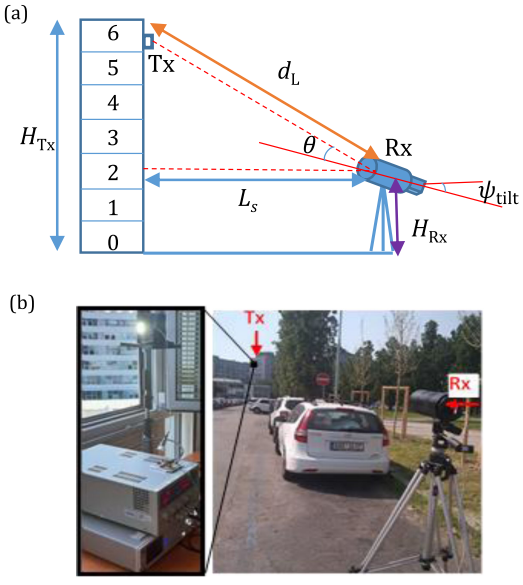

Fig. 6. Proposed OCC link (a) system configuration and (b) experimental setup.

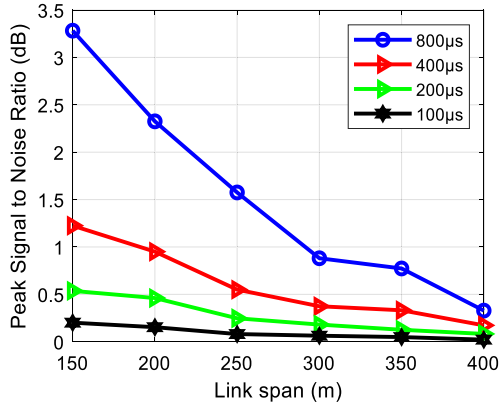

Fig. 7. PSNR versus link span for a range of camera's T_{exp}.

Funding. European Union Horizon 2020 under the Marie Skłodowska Curie grant (764461); Scientific Research Instrument and Equipment, CAS, China (YJKYYQ20170052).

Disclosures. The authors declare no conflicts of interest.

REFERENCES

1. M. J. Jang, *IEEE 802.15 WPAN 15.7 Amendment Study Group* (2019).
2. Z. Ghassemlooy, L. N. Alves, S. Zvanovec, and M.-A. Khalighi, *Visible light communications: Theory and Applications* (CRC Press, 2017).
3. M. K. Hasan, M. Z. Chowdhury, M. Shahjalal, V. T. Nguyen, and Y. M. Jang, Appl. Sci. **8**, 2527 (2018).
4. S. R. Teli, S. Zvanovec, and Z. Ghassemlooy, "Optical Internet of Things within 5G: applications and challenges," in *IEEE International Conference on IoT and Intelligence Systems (IOTAIS)*, Bali, Indonesia, 1 November 2018, pp. 40–45.
5. P. Luo, M. Zhang, Z. Ghassemlooy, H. L. Minh, H. M. Tsai, X. Tang, and D. Han, IEEE Photon. Technol. Lett. **28**, 139 (2016).
6. T. Nguyen, C. H. Hong, N. T. Le, and Y. M. Jang, "High-speed asynchronous optical camera communication using LED and rolling shutter camera," in *2015 Seventh International Conference on Ubiquitous and Future Networks*, Sapporo, Japan, 7 July 2015, pp. 214–219.
7. P. Chavez-Burbano, V. Guerra, J. Rabadan, and R. Perez-Jimenez, "Optical camera communication for smart cities," in *2017 IEEE/CIC International Conference on Communications in China (ICCC Workshops)*, Qingdao, China, 22 October 2017, pp. 1–4.
8. P. Chavez-Burbano, S. Vitek, S. R. Teli, V. Guerra, J. Rabadan, R. Perez-Jimenez, and S. Zvanovec, Electron. Lett. **55**, 334 (2019).
9. E. Eso, Z. Ghassemlooy, S. Zvanovec, A. Gholami, A. Burton, N. B. Hassan, and O. I. Younus, "Experimental demonstration of vehicle to road side infrastructure visible light communications," in *2019 2nd West Asian Colloquium on Optical Wireless Communications (WACOWC)*, Tehran, Iran, 27 April 2019, pp. 85–89.
10. J. M. Kahn and J. R. Barry, Proc. IEEE **85**, 265 (1997).
11. N. B. Hassan, "Mimo visible light communications with camera-based receiver for intelligent transport systems," Ph.D. thesis (Northumbria University, 2019).
12. N. B. Hassan, Y. Huang, Z. Shou, Z. Ghassemlooy, A. Sturniolo, S. Zvanovec, P. Luo, and H. Le-Minh, "Impact of camera lens aperture and the light source size on optical camera communications," in *2018 11th International Symposium on Communication Systems, Networks and Digital Signal Processing (CSNDSP)*, Budapest, Hungary, 18 July 2018, pp. 1–5.
13. S. Verma, "Analysing the performance and stability of LED-to-camera links," Masters thesis (Delft University of Technology, 2017).
14. Q. Huynh-Thu and M. Ghanbari, Electron. Lett. **44**, 800 (2008).